Journal of Computational Physics **164,** 241–257 (2000)
doi:10.1006/jcph.2000.6565, available online at http://www.idealibrary.com on IDEAL®

Compact Finite Difference Schemes for Ocean Models

1. Ocean Waves

Eric Blayo

Projet IDOPT, Laboratoire de Modélisation et Calcul, Université Joseph Fourier, Grenoble, France
E-mail: Eric.Blayo@imag.fr

Received September 15, 1999; revised June 1, 2000

A general framework is derived which leads to generic expressions of discrete dispersion relationships for inertia–gravity and Rossby waves, valid for every finite difference scheme and every type of grid. These relationships are used to investigate the performance of fourth-order and sixth-order compact implicit schemes on Arakawa grids A–E. It is shown that the use of compact schemes leads to very clear improvement in approximating frequency and group velocity of inertia–gravity waves. On the other hand, increasing the order of the schemes does not necessarily improve the accuracy of the discrete dispersion relationship in the case of Rossby waves. Globally, the fourth-order family is found to be a good compromise, which improves significantly the quality of the approximation of the dispersion properties with regard to conventional second-order centered schemes.

Key Words: finite difference approximations; inertia–gravity waves; Rossby waves; oceanography.

1. INTRODUCTION

Numerical models of the ocean circulation have been very much improved these past 15 years, particularly in terms of physics, realism of the applications, and computation techniques. Numerous current models treat the full equations of physical oceanography (the so-called "primitive equations") to simulate the dynamical behavior of the ocean on a basin scale (or even the global ocean) with a high resolution (typically $1/6^\circ$ to $1/10^\circ$ on the horizontal, with tens of vertical levels). The huge computational burden makes it often necessary to run these models on massively parallel supercomputers via domain decomposition techniques.

In this context of rapid improvement, it is striking to note that very few significant modifications occurred in the basic numerics of the models, since the large majority of

0021-9991/00 $35.00

ocean general circulation models still use only simple second-order centered finite difference schemes. However, numerous modern schemes exist that feature interesting properties when compared to conventional schemes. Such is the case, for example, for the implicit schemes based on Hermitian formulas, which is an old idea (e.g., [4]) that became popular in the field of computational fluid dynamics only recently, mostly through the work of Lele [9], under the name of *compact difference* schemes. Note that, in the domain of oceanography, Chu and Fan [3] applied a family of schemes based on such Hermitian formulas (called *combined compact difference* schemes) to the simple stationary Stommel model.

The aim of the present work is to investigate the potential interest of such higher order schemes within the specific context of numerical ocean models. In this first part, we will focus on the representation of inertia–gravity and Rossby waves, which play an important role in the setup of the ocean circulation. Following the studies of Arakawa and Lamb [2], Wajsowicz [11], Fox-Rabinovitz [6], Adcroft [1], and Dukowicz [5], who evaluated the performance of conventional second-order centered schemes in representing these waves on different types of grids, we will derive a general framework allowing a systematic evaluation of the performance of finite difference schemes in this particular context.

This paper is organized as follows. We introduce in Section 2 the 1-D schemes studied in this paper and give some insight into their spectral properties. The 2-D schemes used in the rest of the paper are expressed in Section 3 as functions of the preceding 1-D schemes, for different types of grids. Then the application to the discretization of inertia–gravity (Section 4) and Rossby (Section 5) waves is discussed, and some conclusions are drawn in Section 6.

2. ONE-DIMENSIONAL SCHEMES

To build the 2-D schemes necessary for the discretization of the equations considered in this paper, only three 1-D schemes are necessary. Given the values f_i of a function f on a regular 1-D grid $(x_i)_{i\in N}$, we will define:

- S_0: an interpolation scheme providing estimates $f_{i+1/2}$ of the values of f at the midpoints $x_{i+1/2} = (x_i + x_{i+1})/2$.
- $S_{1/2}$: a scheme providing estimates $f'_{i+1/2}$ of the first derivative f' at points $x_{i+1/2}$.
- S_1: a scheme providing estimates f'_i of the first derivative f' at points x_i.

In the present study, we decided to focus on schemes of practical interest in the context of oceanography and to limit ourselves to schemes using only gridpoints within one mesh around the current gridpoint. This is what is done in most ocean models, in order to limit the problems of numerical diffusion and of deriving noncentered schemes near the boundaries. It led us to the selection of three families of schemes.

The first one is composed of explicit second-order centered schemes (E2S), which are the schemes conventionally used in ocean circulation models. The second family is based on fourth-order compact schemes (C4S), as presented for example in [9]. The third family is composed of sixth-order compact schemes (C6S). Note that, to avoid the use of gridpoints more than one mesh away from the current gridpoint, the scheme S_1 in this third family requires the simultaneous estimation of the first and the second derivatives (see [3] for more details on this particular scheme). These three families are listed in Table I. A thorough comparison of the properties of the compact schemes with classical explicit higher order schemes can be found in [9].

TABLE I
The Three Families of 1-D Schemes

	Scheme
E2S	
S_0	$f_{i+1/2} = \frac{1}{2}(f_i + f_{i+1})$
$S_{1/2}$	$f'_{i+1/2} = \frac{f_{i+1} - f_i}{d}$
S_1	$f'_i = \frac{f_{i+1} - f_{i-1}}{2d}$
C4S	
S_0	$\frac{1}{6} f_{i-1/2} + f_{i+1/2} + \frac{1}{6} f_{i+3/2} = \frac{2}{3}(f_i + f_{i+1})$
$S_{1/2}$	$\frac{1}{22} f'_{i-1/2} + f'_{i+1/2} + \frac{1}{22} f'_{i+3/2} = \frac{12}{11}\frac{f_{i+1} - f_i}{d}$
S_1	$\frac{1}{4} f'_{i-1} + f'_i + \frac{1}{4} f'_{i+1} = \frac{3}{2}\frac{f_{i+1} - f_{i-1}}{2d}$
C6S	
S_0	$\frac{3}{10} f_{i-1/2} + f_{i+1/2} + \frac{3}{10} f_{i+3/2} = \frac{3}{4}(f_i + f_{i+1}) + \frac{1}{20}(f_{i-1} + f_{i+2})$
$S_{1/2}$	$\frac{9}{62} f'_{i-1/2} + f'_{i+1/2} + \frac{9}{62} f'_{i+3/2} = \frac{63}{62}\frac{f_{i+1} - f_i}{d} + \frac{17}{62}\frac{f_{i+2} - f_{i-1}}{3d}$
S_1	$\begin{cases} f'_i + \frac{7}{16}(f'_{i+1} + f'_{i-1}) - \frac{d}{16}(f''_{i+1} - f''_{i-1}) = \frac{15}{16d}(f_{i+1} - f_{i-1}) \\ f''_i - \frac{1}{8}(f''_{i+1} + f''_{i-1}) + \frac{9}{8d}(f'_{i+1} - f'_{i-1}) = \frac{3}{d^2}(f_{i+1} - 2f_i + f_{i-1}) \end{cases}$

Note. d is the grid spacing.

To quantify and compare the properties of these different 1-D schemes, we have calculated their *transfer functions* (TFs), which are summarized in Table II. We remind the reader that the transfer function T of a scheme S is defined by $S(e^{ikx}) = T(k)e^{ikx}$ and gives insight into the spectral resolution of S. These TFs are compared in Fig. 1 to the TF of the exact interpolation and derivative operators, which clearly illustrates the better approximation properties of C4S and C6S with regard to E2S.

We have also reported in Table II a *first-order TF* for $S_{1/2}$ and S_1. This function R is needed for the study of the approximation of Rossby waves (see Section 5) and is defined by $S[(x - x_0)e^{ikx}](x_0) = R(k)e^{ikx_0}$ for any x_0.

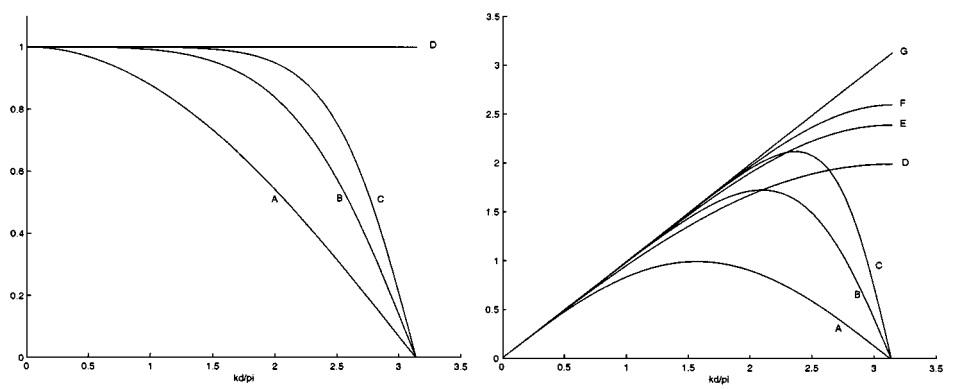

FIG. 1. Transfer functions of exact and approximate operators described in Table II. Left: T_0 for E2S (A), C4S (B), C6S (C) and exact interpolation (D). Right: T_1 for E2S (A), C4S (B), C6S (C); $T_{1/2}$ for E2S (D), C4S (E), C6S (F), and exact derivation (G).

TABLE II
Zero-Order and First-Order Transfer Functions of the Three Families of 1-D Schemes and of the Exact Operators

Scheme	Transfer function $T(k)$	First-order transfer function $R(k)$
Exact		
Interpolation	$T_0(k) = 1$	$R_0(k) = 0$
Derivation	$T(k) = ik$	$R(k) = 1$
E2S		
S_0	$T_0(k) = \cos\frac{kd}{2}$	$R_0(k) = \frac{id}{2}\sin\frac{kd}{2}$
$S_{1/2}$	$T_{1/2}(k) = \frac{2i}{d}\sin\frac{kd}{2}$	$R_{1/2}(k) = \cos\frac{kd}{2}$
S_1	$T_1(k) = \frac{i}{d}\sin kd$	$R_1(k) = \cos kd$
C4S		
S_0	$T_0(k) = \frac{4\cos(kd/2)}{3+\cos kd}$	$R_0(k) = \frac{id}{2}\frac{4\sin(kd/2)}{3+\cos kd}$
$S_{1/2}$	$T_{1/2}(k) = \frac{2i}{d}\frac{12\sin(kd/2)}{11+\cos kd}$	$R_{1/2}(k) = \frac{12\cos(kd/2)}{11+\cos kd}$
S_1	$T_1(k) = \frac{i}{d}\frac{3\sin kd}{2+\cos kd}$	$R_1(k) = \frac{3\cos kd}{2+\cos kd}$
C6S		
S_0	$T_0(k) = \frac{15\cos(kd/2)+\cos(3kd/2)}{10+6\cos kd}$	$R_0(k) = \frac{id}{2}\frac{15\sin(kd/2)+3\sin(3kd/2)}{10+6\cos kd}$
$S_{1/2}$	$T_{1/2}(k) = \frac{2i}{d}\frac{63\sin(kd/2)+\frac{17}{3}\sin(3kd/2)}{62+18\cos kd}$	$R_{1/2}(k) = \frac{63\cos(kd/2)+17\cos(3kd/2)}{62+18\cos kd}$
S_1	$T_1(k) = \frac{i}{d}\frac{9(4+\cos kd)\sin kd}{23+20\cos kd+2\cos^2 kd}$	$R_1(k) = \frac{-24+60\cos kd+9\cos^2 kd}{23+20\cos kd+2\cos^2 kd}$

3. LINKS WITH TWO-DIMENSIONAL SCHEMES

Following the well-known Arakawa classification, we will consider the discretization of the shallow water equations on grids of type A to E (Fig. 2), which differ in the location of the discrete variables u, v, and h, where u and v are the horizontal velocity components

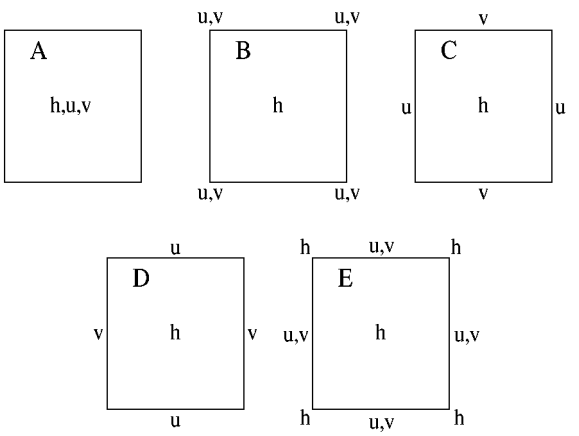

FIG. 2. Grids of type A to E, following Arakawa's classification. Note that the grid spacing is d for grids A–D, and $d\sqrt{2}$ for grid E, in order to have the same distance d between corresponding grid points.

TABLE III
2-D Schemes as Combinations of 1-D Schemes for A to E Grids

	A	B	C	D	E
$\mathcal{S}_0$	Id	Id	$S_0^x \circ S_0^y$	$S_0^x \circ S_0^y$	Id
$\mathcal{S}_x^u$	S_1^x	$S_{1/2}^x \circ S_0^y$	$S_{1/2}^x$	$S_1^x \circ S_0^y$ (or $S_{1/2}^x \circ S_0^x \circ S_0^y$)	$S_{1/2}^x$
$\mathcal{S}_y^v$	S_1^y	$S_{1/2}^y \circ S_0^x$	$S_{1/2}^y$	$S_1^y \circ S_0^x$ (or $S_{1/2}^y \circ S_0^y \circ S_0^x$)	$S_{1/2}^y$

Note. The superscript x or y indicates the direction in which the 1-D scheme is applied.

and h is the displacement from a constant depth H. The inertia–gravity and Rossby waves equations will require the approximation of

- v and $\partial_x h$ at a u-point,
- u and $\partial_y h$ at a v-point, and
- $\partial_x u$ and $\partial_y v$ at an h-point.

By symmetry, we can see that we need, for all grid types, three 2-D schemes:

- $\mathcal{S}_0$ to approximate u at a v-point (and v at a u-point),
- $\mathcal{S}_x^u$ to approximate $\partial_x h$ at a u-point (and $\partial_x u$ at an h-point), and
- $\mathcal{S}_y^v$ to approximate $\partial_y h$ at a v-point (and $\partial_y v$ at an h-point).

These schemes can all be obtained by simple combinations of the preceding 1-D schemes S_0, $S_{1/2}$, and S_1, as indicated in Table III. Note that, for the D-grid, alternative combinations (added in parentheses) could also be considered for $\mathcal{S}_x^u$ and $\mathcal{S}_y^v$. However, they are exactly equivalent for E2S and lead to slightly less compact calculations for C4S and C6S.

The TF of a 2-D scheme being defined by $\mathcal{S}(e^{i(kx+ly)}) = \mathcal{T}(k,l)e^{i(kx+ly)}$, we can easily derive from Table III the expressions for the TFs $\mathcal{T}_0$, $\mathcal{T}_x^u$, and $\mathcal{T}_y^v$ of the 2-D schemes as functions of T_0, $T_{1/2}$, and T_1 (Table IV). We have also derived the expression for $\mathcal{R}_x^u$ and $\mathcal{R}_y^v$, defined by

$$\left.\begin{aligned} \mathcal{S}_x^u\big((y-y_0)e^{i(kx+ly)}\big)(x_0,y_0) &= \mathcal{R}_x^u(k,l)e^{i(kx_0+ly_0)} \\ \mathcal{S}_y^v\big((y-y_0)e^{i(kx+ly)}\big)(x_0,y_0) &= \mathcal{R}_y^v(k,l)e^{i(kx_0+ly_0)} \end{aligned}\right\} \quad \forall (x_0,y_0), \tag{1}$$

as a function of T_0, R_0, $T_{1/2}$, $R_{1/2}$, T_1, and R_1. $\mathcal{R}_x^u$ and $\mathcal{R}_y^v$ will be useful in Section 5.

TABLE IV
2-D Transfer Functions as Combinations of 1-D Transfer Functions for A to E Grids

	A	B	C	D	E
$\mathcal{T}_0(k,l)$	1	1	$T_0(k)T_0(l)$	$T_0(k)T_0(l)$	1
$\mathcal{T}_x^u(k,l)$	$T_1(k)$	$T_{1/2}(k)T_0(l)$	$T_{1/2}(k)$	$T_1(k)T_0(l)$	$T_{1/2}(k)$
$\mathcal{T}_y^v(k,l)$	$T_1(l)$	$T_0(k)T_{1/2}(l)$	$T_{1/2}(l)$	$T_0(k)T_1(l)$	$T_{1/2}(l)$
$\mathcal{R}_x^u(k,l)$	0	$T_{1/2}(k)R_0(l)$	0	$T_1(k)R_0(l)$	0
$\mathcal{R}_y^v(k,l)$	$R_1(l)$	$T_0(k)R_{1/2}(l)$	$R_{1/2}(l)$	$T_0(k)R_1(l)$	$R_{1/2}(l)$

4. INERTIA–GRAVITY WAVES

4.1. *Continuous Equations*

Inertia–gravity waves on an f-plane are described by the linearized shallow-water equations (e.g., [7])

$$\begin{aligned} \partial_t u - f_0 v + g\partial_x h &= 0 \\ \partial_t v + f_0 u + g\partial_y h &= 0 \\ \partial_t h + H(\partial_x u + \partial_y v) &= 0, \end{aligned} \tag{2}$$

where f_0 is the Coriolis parameter (assumed constant) and g is the gravity acceleration. Assuming plane waves of the form

$$(u, v, h) = (U_0, V_0, H_0)\, e^{i(kx+ly-\omega t)}, \tag{3}$$

Equation (2) becomes

$$\begin{aligned} -i\omega U_0 - f_0 V_0 + ikgH_0 &= 0 \\ -i\omega V_0 + f_0 U_0 + ilgH_0 &= 0 \\ -i\omega H_0 + iH(kU_0 + lV_0) &= 0, \end{aligned} \tag{4}$$

which leads to the well-known dispersion relationship

$$\left(\frac{\omega}{f_0}\right)^2 = 1 + \lambda^2(k^2 + l^2), \tag{5}$$

where $\lambda = \sqrt{gH}/f_0$ is the Rossby radius of deformation.

4.2. *Discrete Dispersion Relationship*

The semi-discretized system analogous to system (2) is

$$\begin{aligned} \partial_t u - f_0 \mathcal{S}_0(v) + g\mathcal{S}_x^u(h) &= 0 \\ \partial_t v + f_0 \mathcal{S}_0(u) + g\mathcal{S}_y^v(h) &= 0 \\ \partial_t h + H\left[\mathcal{S}_x^u(u) + \mathcal{S}_y^v(v)\right] &= 0, \end{aligned} \tag{6}$$

which becomes, with the plane wave approximation (3),

$$\begin{aligned} -i\omega U_0 - f_0 V_0 \mathcal{T}_0(k,l) + gH_0 \mathcal{T}_x^u(k,l) &= 0 \\ -i\omega V_0 + f_0 U_0 \mathcal{T}_0(k,l) + gH_0 \mathcal{T}_y^v(k,l) &= 0 \\ -i\omega H_0 + H\left[U_0 \mathcal{T}_x^u(k,l) + V_0 \mathcal{T}_y^v(k,l)\right] &= 0. \end{aligned} \tag{7}$$

This leads to the discrete dispersion relationship

$$\left(\frac{\omega}{f_0}\right)^2 = \mathcal{T}_0^2(k,l) - \lambda^2\left[\mathcal{T}_x^u(k,l)^2 + \mathcal{T}_y^v(k,l)^2\right]. \tag{8}$$

Note that this relationship reduces to the exact relationship (5) in the limit case of perfect

discrete schemes, since in that case the TF of the interpolation operator is the constant function 1, and the TF of the derivatives in x and y are respectively ik and il.

The relationship (8) can be expanded for each grid using Table III:

$$
\begin{aligned}
&\text{A:} \quad \left(\frac{\omega}{f}\right)^2 = 1 - \lambda^2\left[T_1^2(k) + T_1^2(l)\right] \\
&\text{B:} \quad \left(\frac{\omega}{f}\right)^2 = 1 - \lambda^2\left[T_{1/2}^2(k)T_0^2(l) + T_{1/2}^2(l)T_0^2(k)\right] \\
&\text{C:} \quad \left(\frac{\omega}{f}\right)^2 = T_0^2(k)T_0^2(l) - \lambda^2\left[T_{1/2}^2(k) + T_{1/2}^2(l)\right] \\
&\text{D:} \quad \left(\frac{\omega}{f}\right)^2 = T_0^2(k)T_0^2(l) - \lambda^2\left[T_1^2(k)T_0^2(l) + T_0^2(k)T_1^2(l)\right] \\
&\text{E:} \quad \left(\frac{\omega}{f}\right)^2 = 1 - \lambda^2\left[T_{1/2}^2(k) + T_{1/2}^2(l)\right].
\end{aligned}
\tag{9}
$$

Note that the valid phase space in the case of the E grid is different from those for the other grids (see Fig. 2).

4.3. *Application to Explicit and Compact Schemes*

We compared the discrete dispersion relationships (9) to the exact continuous relationship (5) for the three different families of schemes listed in Table I. The corresponding curves are displayed in Figs. 3 and 4 for each type of grid, both in a resolved ($\lambda/d = 2$) and in an under-resolved ($\lambda/d = 0.25$) case. They represent the relative frequency error $(\omega^{\text{num}} - \omega)/\omega$ for wavelengths greater than $2d$. Such a comparison was already performed for E2S by several authors; e.g., [5, 11]. They demonstrated that the A and D grids are not suitable for representing these waves because the numerical modes create "null spaces" effects. (Numerical frequency systematically decreases to 1 or even 0 at points $(k, l) = (0, \pi/d)$ or $(\pi/d, 0)$.) In contrast, the B and C grids are suitable for representing these waves; the B grid is more accurate than the C grid in the resolved case ($\lambda > d$) and less accurate in the under-resolved case ($\lambda < d$).

Given the expressions in (9), it is clear that the better the TFs of the schemes the better the approximation of ω (and hence of the phase velocity $[\omega/k, \omega/l]$). Therefore, the approximation of ω should be improved with the order of the schemes. Figures 3 and 4 illustrate exactly this behavior. The use of C4S and C6S systematically improves the accuracy of the numerical frequency, often in a quite spectacular way. The fact that the C grid gives the best results in the resolved case, while it is the B grid in the under-resolved case, remains valid for the compact schemes. However, the domain of accuracy is very much enlarged with C4S or C6S in comparison to E2S, and both B and C grids are probably good choices with those compact schemes, whatever the grid resolution. Note also that the suitability of the grids (and in particular the null spaces effects in the A and D grids) remains unchanged.

This investigation can be complemented by computing the discrete group velocities $(\partial\omega/\partial k, \partial\omega/\partial l)$, as done, for example, by Song and Tang [10] and Haidvogel and Beckmann [8] for E2S. As a matter of fact, numerical effects (in particular spurious modes) can have a negative impact on the group velocity which can take locally very false values or even the wrong sign. It has been shown, for example, that the C grid gives unreasonable group velocity in the under-resolved case, even for very small wave numbers. The errors in group

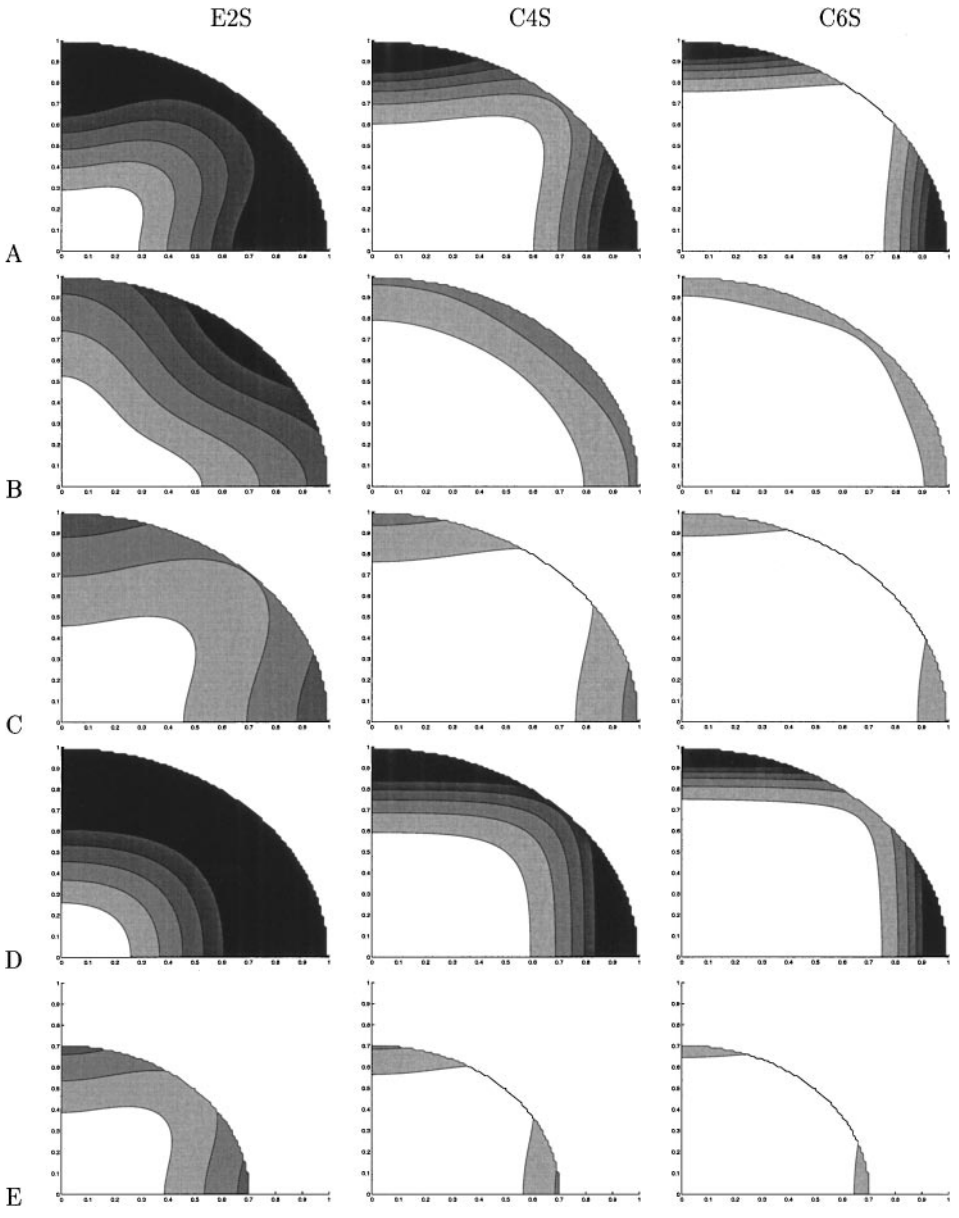

FIG. 3. Inertia–gravity waves: rms error on ω as a function of kd/π and ld/π for A to E grids and for the three families of schemes ($\lambda/d = 2$). Contour values are 10, 20, 30, 40, and 50% (from white to black). Due to the symmetry of the problem, only the upper right quadrant is shown.

velocity amplitudes $(|c_g|^{\text{num}} - |c_g|)/|c_g|$ are shown in Figs. 5 and 6, as well as error vectors when the numerical group velocity departs from the exact analytical one by more than 30°. We can observe behavior similar to that in the dispersion analysis, i.e., a very clear improvement of the accuracy of the numerical approximations when compact schemes are used, in terms both of amplitude and of direction of the group velocity. In particular, both B and C grids lead to rather good results, the B grid being, however, still better than the C grid in the under-resolved case. Note also, as previously mentioned, that the compact schemes do not remove the grid-dependent numerical modes.

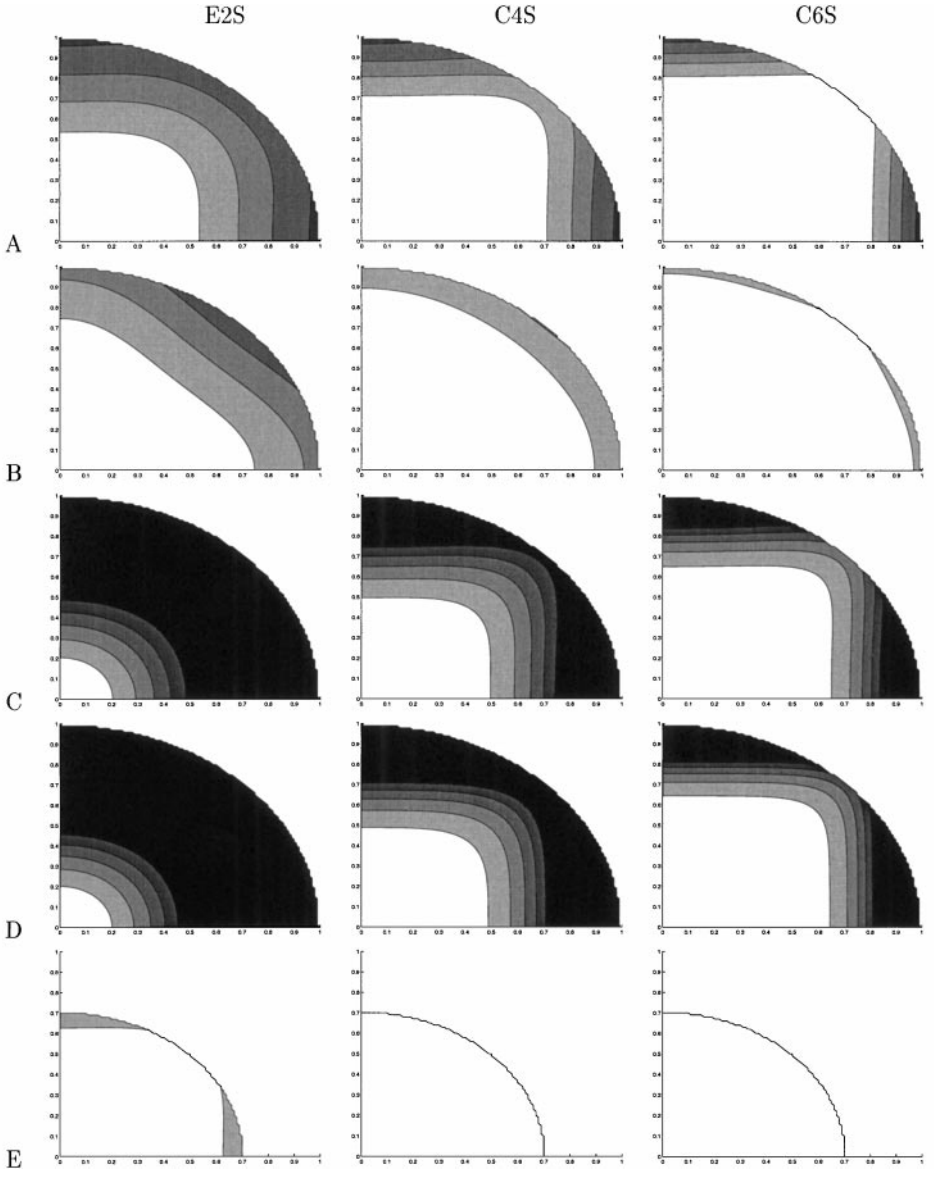

FIG. 4. Same as Fig. 3, for $\lambda/d = 0.25$. Contour values are 5, 10, 15, 20, and 25%.

5. ROSSBY WAVES

5.1. *Continuous Equations*

The equations for Rossby waves in the linearized and β-plane approximation are (e.g., [7])

$$\begin{aligned} f_0 v_g - g\partial_x h_g &= 0 \\ f_0 u_g + g\partial_y h_g &= 0 \\ \partial_t u_g - f_0 v_a - \beta y v_g &= 0 \\ \partial_t v_g + f_0 u_a + \beta y u_g &= 0 \\ \partial_t h_g + H\left(\partial_x u_a + \partial_y v_a\right) &= 0. \end{aligned} \tag{10}$$

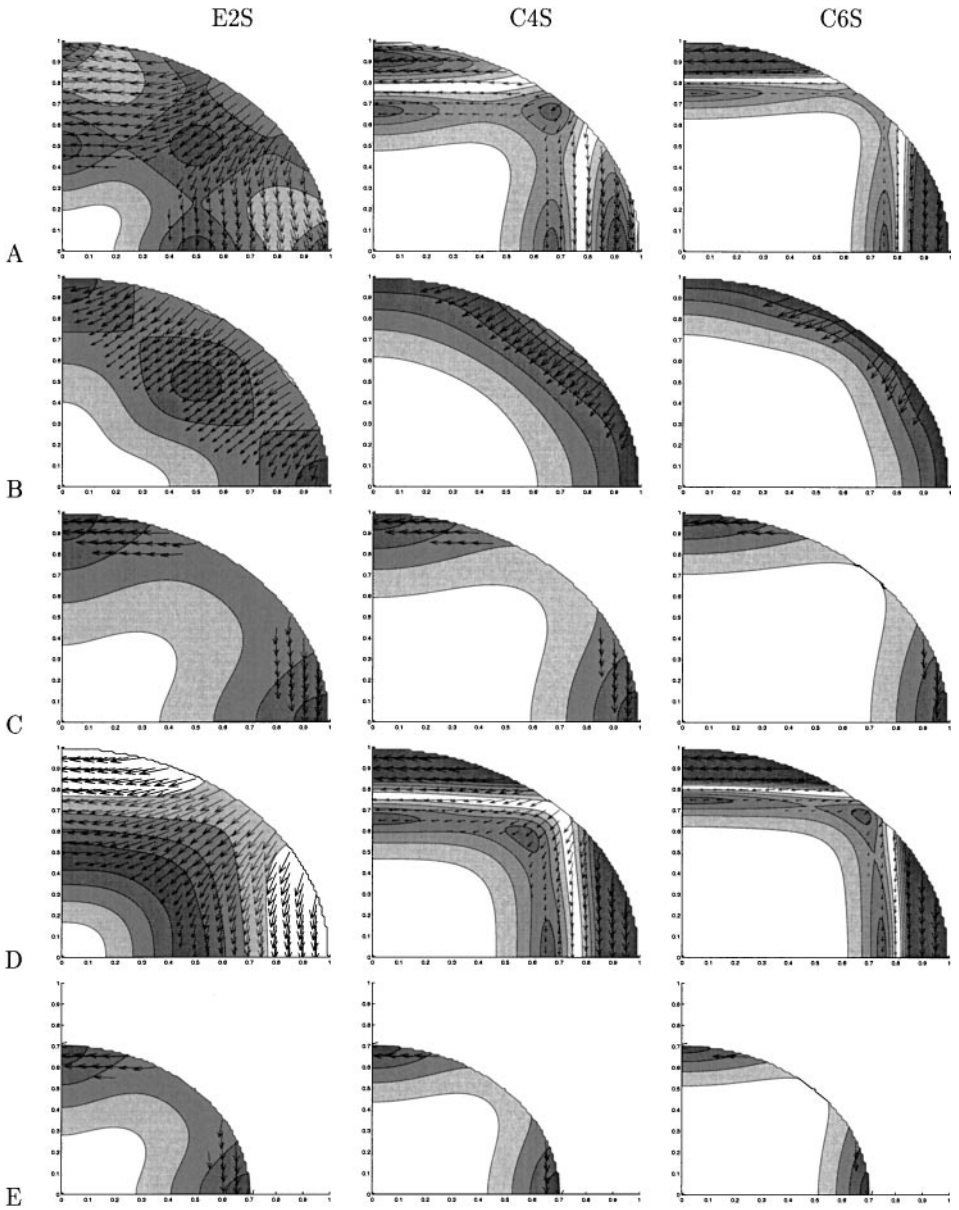

FIG. 5. Group velocity amplitude rms error corresponding to Fig. 3. Contour values are 20, 40, 60, 80, and 100%. Error vectors are plotted when the angle between exact and discrete group velocities is greater than 30°.

The subscripts g and a denote the geostrophic and ageostrophic components. The Coriolis parameter depends linearly on y: $f = f_0 + \beta y$, with f_0 and β constant. Assuming plane-wave solutions of the form (note that U_g, V_g, and H_g are constant, while U_a and V_a must depend on y)

$$\begin{pmatrix} u_g(x,y,t) \\ v_g(x,y,t) \\ u_a(x,y,t) \\ v_a(x,y,t) \\ h_g(x,y,t) \end{pmatrix} = \begin{pmatrix} U_g \\ V_g \\ U_a(y) \\ V_a(y) \\ H_g \end{pmatrix} e^{i(kx+ly-\omega t)}, \tag{11}$$

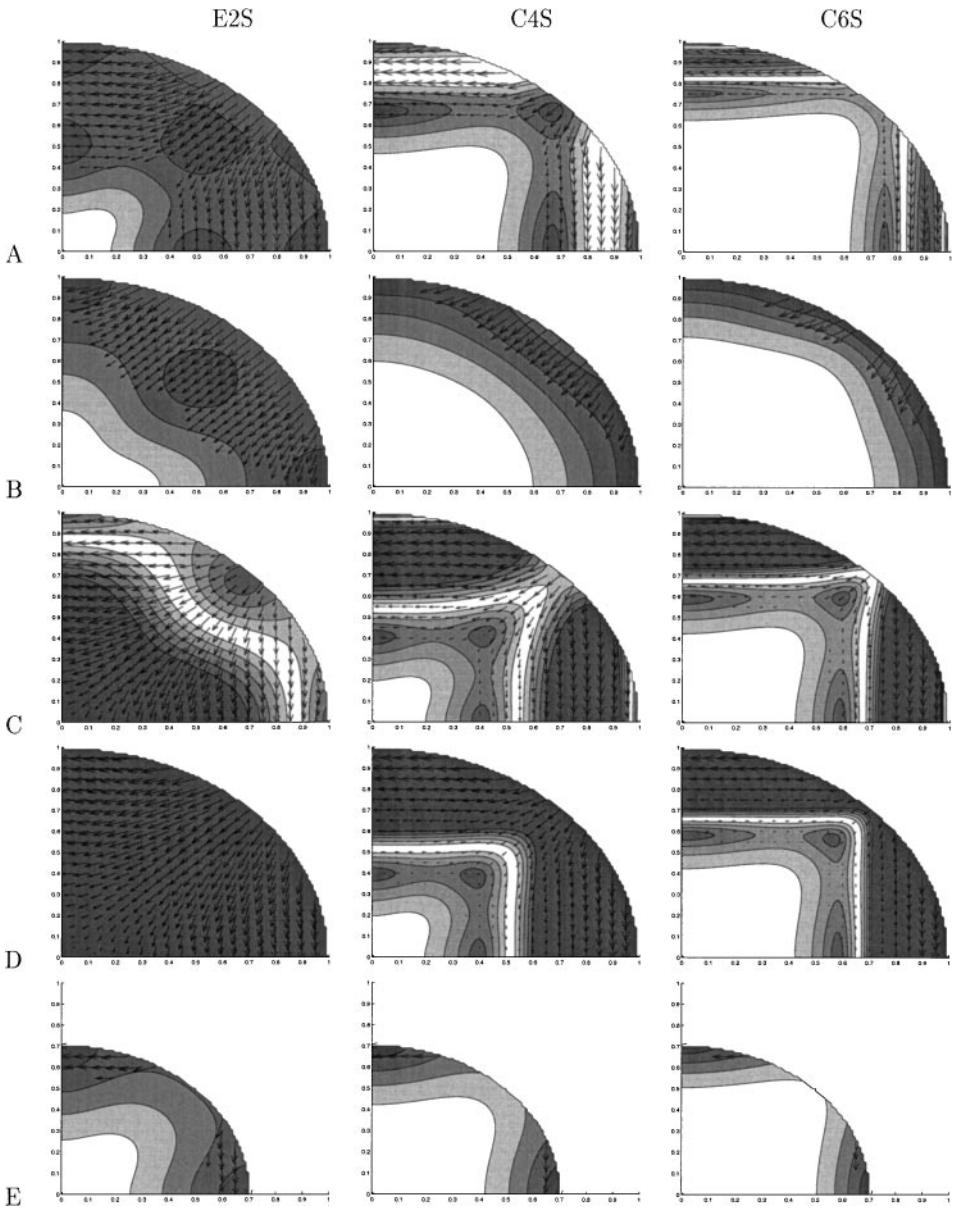

FIG. 6. Same as Fig. 5, for $\lambda/d = 0.25$.

system (10) becomes

$$\begin{aligned} f_0 V_g - ikgH_g &= 0 \\ f_0 U_g + ilgH_g &= 0 \\ -i\omega U_g - f_0 V_a - \beta y V_g &= 0 \\ -i\omega V_g + f_0 U_a + \beta y U_g &= 0 \\ -i\omega H_g + H(ikU_a + ilV_a + \partial_y V_a) &= 0. \end{aligned} \tag{12}$$

Hence, after elimination, the dispersion relationship is

$$\frac{\omega}{\beta} = \frac{-\lambda^2 k}{1 + \lambda^2(k^2 + l^2)}. \tag{13}$$

5.2. *Discrete Dispersion Relationship*

The semi-discretized system analogous to system (10) is

$$f_0\mathcal{S}_0(v_g) - g\mathcal{S}_x^u(h_g) = 0 \tag{14a}$$
$$f_0\mathcal{S}_0(u_g) + g\mathcal{S}_y^v(h_g) = 0 \tag{14b}$$
$$\partial_t u_g - f_0\mathcal{S}_0(v_a) - \beta y\mathcal{S}_0(v_g) = 0 \tag{14c}$$
$$\partial_t v_g + f_0\mathcal{S}_0(u_a) + \beta y\mathcal{S}_0(u_g) = 0 \tag{14d}$$
$$\partial_t h_g + H\left[\mathcal{S}_x^u(u_a) + \mathcal{S}_y^v(v_a)\right] = 0. \tag{14e}$$

Making the assumption (11) of a discrete plane-wave solution, (14a) and (14b) become

$$U_g = -\frac{g}{f_0}\,\frac{\mathcal{T}_y^v(k,l)}{\mathcal{T}_0(k,l)}\,H_g \quad \text{and} \quad V_g = \frac{g}{f_0}\,\frac{\mathcal{T}_x^u(k,l)}{\mathcal{T}_0(k,l)}\,H_g, \tag{15}$$

while (14c) and (14d) give expressions for $\mathcal{S}_0(u_a)$ and $\mathcal{S}_0(v_a)$:

$$\mathcal{S}_0(u_a) = \frac{g}{f_0^2}H_g\left[i\omega\frac{\mathcal{T}_x^u(k,l)}{\mathcal{T}_0(k,l)} + \beta y\mathcal{T}_y^v(k,l)\right]e^{i(kx+ly-\omega t)} \tag{16a}$$
$$\mathcal{S}_0(v_a) = \frac{g}{f_0^2}H_g\left[i\omega\frac{\mathcal{T}_y^v(k,l)}{\mathcal{T}_0(k,l)} - \beta y\mathcal{T}_x^u(k,l)\right]e^{i(kx+ly-\omega t)}. \tag{16b}$$

Hence, applying scheme $\mathcal{S}_0$ to (14e) gives

$$\partial_t\mathcal{S}_0(h_g) + H\left[\mathcal{S}_0\circ\mathcal{S}_x^u(u_a) + \mathcal{S}_0\circ\mathcal{S}_y^v(v_a)\right] = 0. \tag{17}$$

Notice that $\mathcal{S}_0$ commutes with $\mathcal{S}_x^u$ and $\mathcal{S}_y^v$ due to the particular structure of the corresponding matrices (symmetric Toeplitz, i.e., constant coefficient on each diagonal) and that $\mathcal{S}(ye^{i(kx+ly-\omega t)}) = [\mathcal{R}(k,l) + y\mathcal{T}(k,l)]e^{i(kx+ly-\omega t)}$ ($\mathcal{R}$ being defined by (1) at the end of Section 3). Then introducing (16a) and (16b), (17) becomes after a little algebra

$$\frac{\omega}{\beta} = i\lambda^2\,\mathcal{T}_0(k,l)\frac{\mathcal{T}_x^u(k,l)\mathcal{R}_y^v(k,l) - \mathcal{T}_y^v(k,l)\mathcal{R}_x^u(k,l)}{\mathcal{T}_0(k,l)^2 - \lambda^2\left[\mathcal{T}_x^u(k,l)^2 + \mathcal{T}_y^v(k,l)^2\right]}. \tag{18}$$

We can of course verify that the exact dispersion relationship (13) can be retrieved in the limit case of perfect discrete operators, since in that case $\mathcal{T}_0(k,l)$, $\mathcal{T}_x^u(k,l)$, $\mathcal{T}_y^v(k,l)$, $\mathcal{R}_x^u(k,l)$, and $\mathcal{R}_y^v(k,l)$ are respectively equal to 1, ik, il, 0, and 1.

This relationship (18) can be developed using Table IV for each type of grid:

A: $$\frac{\omega}{\beta} = i\lambda^2\frac{T_1(k)R_1(l)}{1-\lambda^2\left[T_1^2(k)+T_1^2(l)\right]} \tag{19a}$$

B: $$\frac{\omega}{\beta} = i\lambda^2\frac{T_0(k)T_{1/2}(k)\left[T_0(l)R_{1/2}(l) - T_{1/2}(l)R_0(l)\right]}{1-\lambda^2\left[T_0^2(k)T_{1/2}^2(l) + T_0^2(l)T_{1/2}^2(k)\right]} \tag{19b}$$

C: $$\frac{\omega}{\beta} = i\lambda^2\frac{T_0(k)T_{1/2}(k)T_0(l)R_{1/2}(l)}{T_0^2(k)T_0^2(l) - \lambda^2\left[T_{1/2}^2(k)+T_{1/2}^2(l)\right]} \tag{19c}$$

$$\text{D:}\qquad \frac{\omega}{\beta} = i\lambda^2 \frac{T_0^2(k)T_1(k)T_0(l)[T_0(l)R_1(l) - T_1(l)R_0(l)]}{T_0^2(k)T_0^2(l) - \lambda^2\left[T_1^2(k)T_0^2(l) + T_0^2(k)T_1^2(l)\right]} \tag{19d}$$

$$\text{E:}\qquad \frac{\omega}{\beta} = i\lambda^2 \frac{T_{1/2}(k)R_{1/2}(l)}{1 - \lambda^2\left[T_{1/2}^2(k) + T_{1/2}^2(l)\right]} \tag{19e}$$

5.3. *Application to Explicit and Compact Schemes*

As for inertia–gravity waves, we plotted for each type of grid and each family of schemes the relative frequency error (Figs. 7 and 8) and the group velocity error (Figs. 9 and 10). Surprisingly, unlike the previous results concerning inertia–gravity waves, the approximations

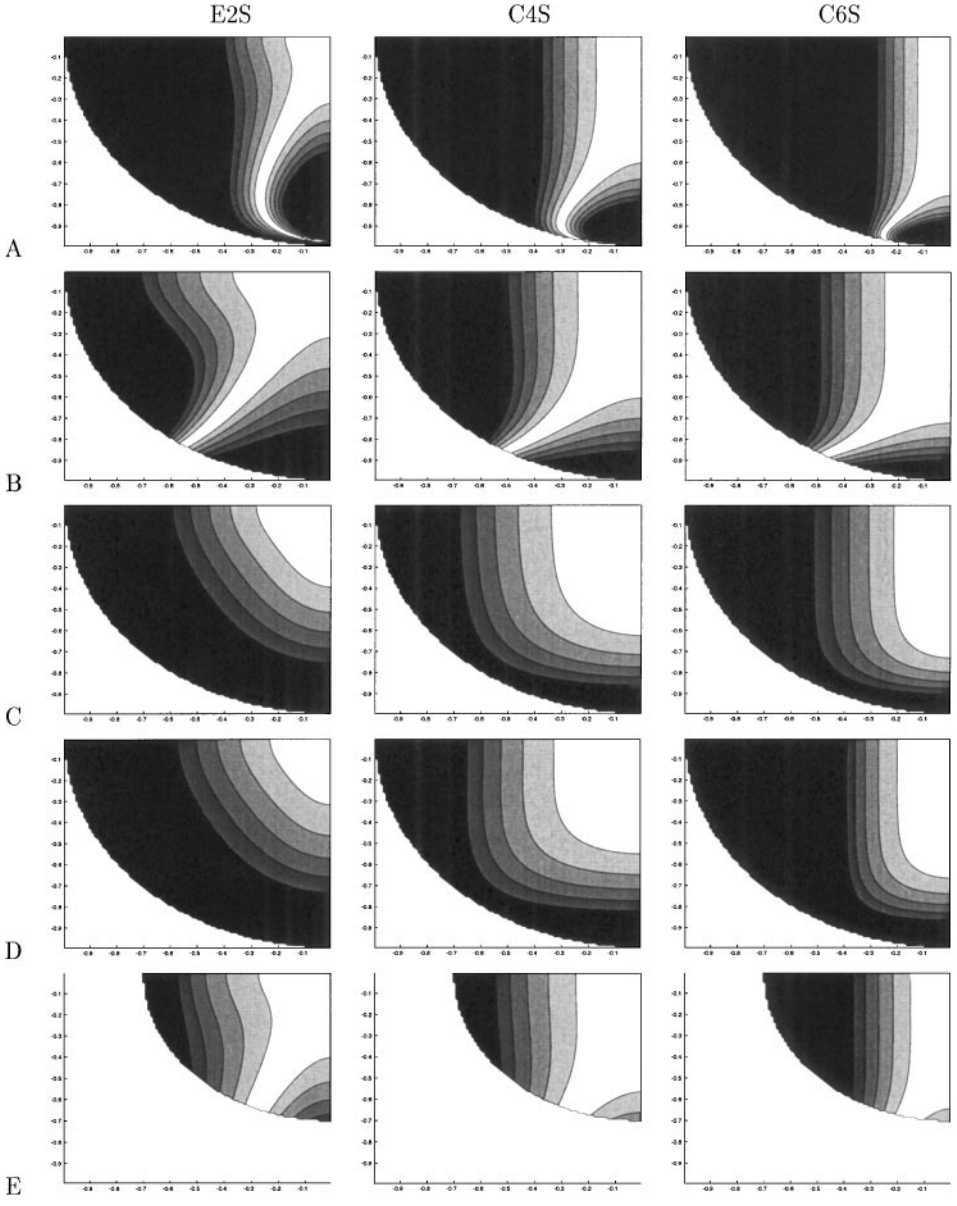

FIG. 7. Same as Fig. 3, but for Rossby waves. Contour values are 10, 20, 30, 40, and 50%.

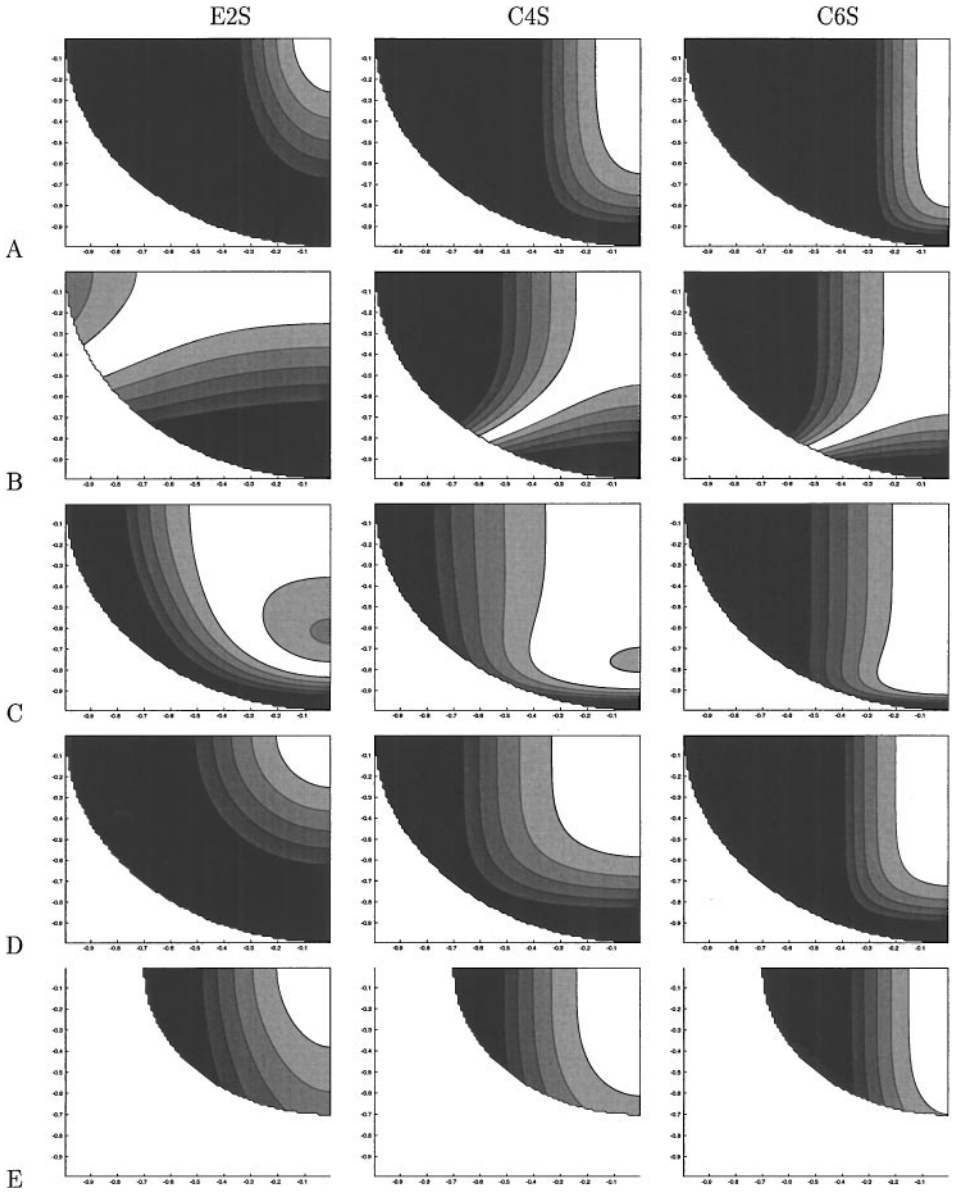

FIG. 8. Same as Fig. 7, for $\lambda/d = 0.25$.

are not systematically improved when the order of the schemes increases. It is even rather clear that the use of C6S often leads to poorer results than with C4S, especially in the under-resolved case.

This can be easily explained by the form of the discrete relationship (18), which involves not only the TFs T of the schemes but also the first-order TFs R. We have plotted these first-order TFs on Fig. 11, and it is striking to see that the quality of R systematically decreases with the order of the schemes, especially for high wave numbers. The only exceptions are that $R_{1/2}$ is better for C4S than for E2S for all wave numbers and that R_1 is better for C4S than for E2S for short and intermediate wave numbers. Thus the changes in the approximation of the frequency and the group velocity that occur when the order of the

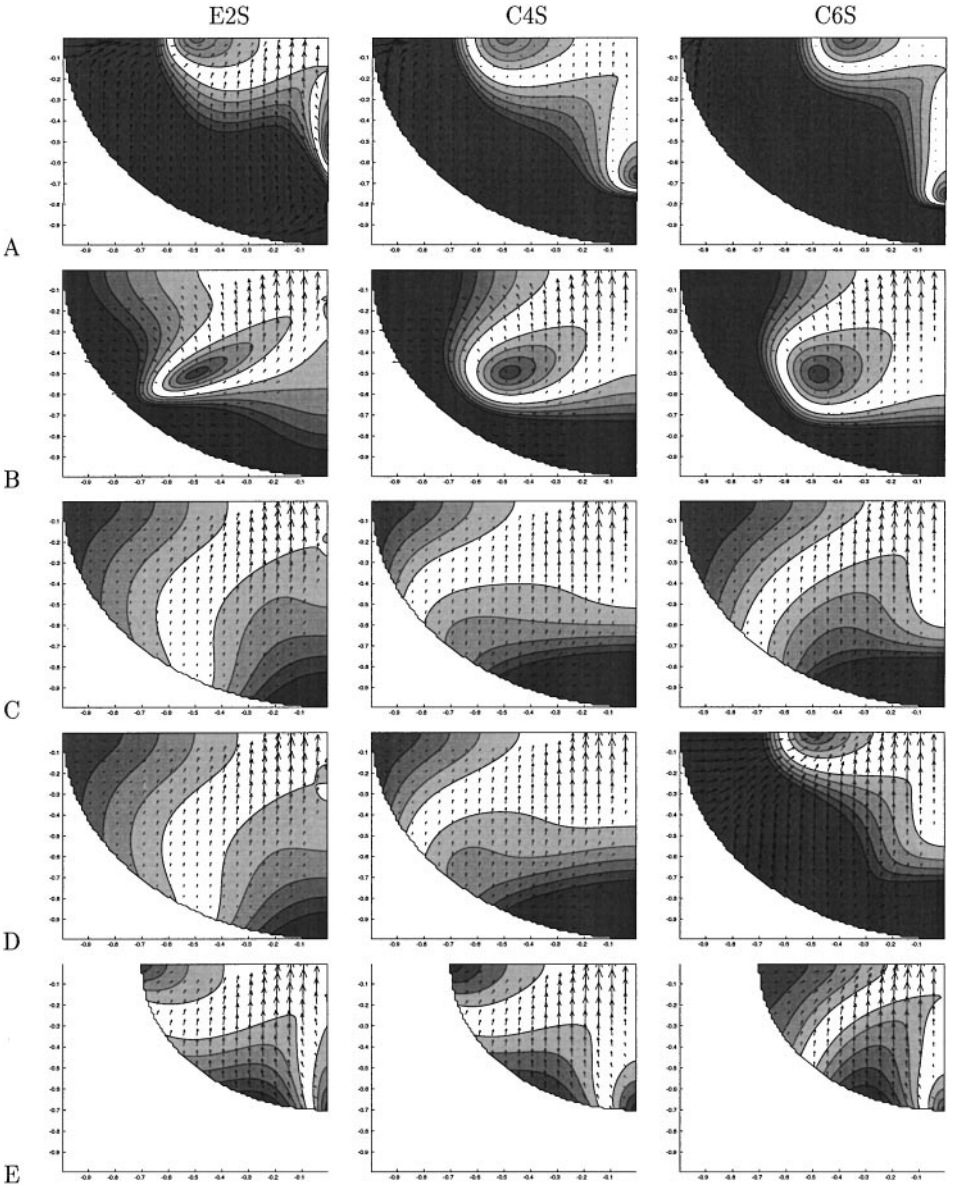

FIG. 9. Same as Fig. 5, but for Rossby waves.

schemes is increased result in most cases from a compromise between improving T and making R worse. Moreover the Rossby wave frequency appears as a ratio, and improving both the numerator and the denominator of (18) will not necessarily improve the ratio itself.

Globally, the approximations are better for C4S than for E2S. This is particularly clear for the C grid, which does not involve R_0 or R_1, and for the D grid. For the B grid, the performance with C4S remains globally unchanged with regard to E2S, except that the group velocity error decreases and becomes more isotropic with C4S in the under-resolved case. On the other hand, the use of C6S often leads to poorer results than with C4S, mostly for intermediate and large wave numbers. Thus the C4S family is probably the best choice for representing Rossby waves.

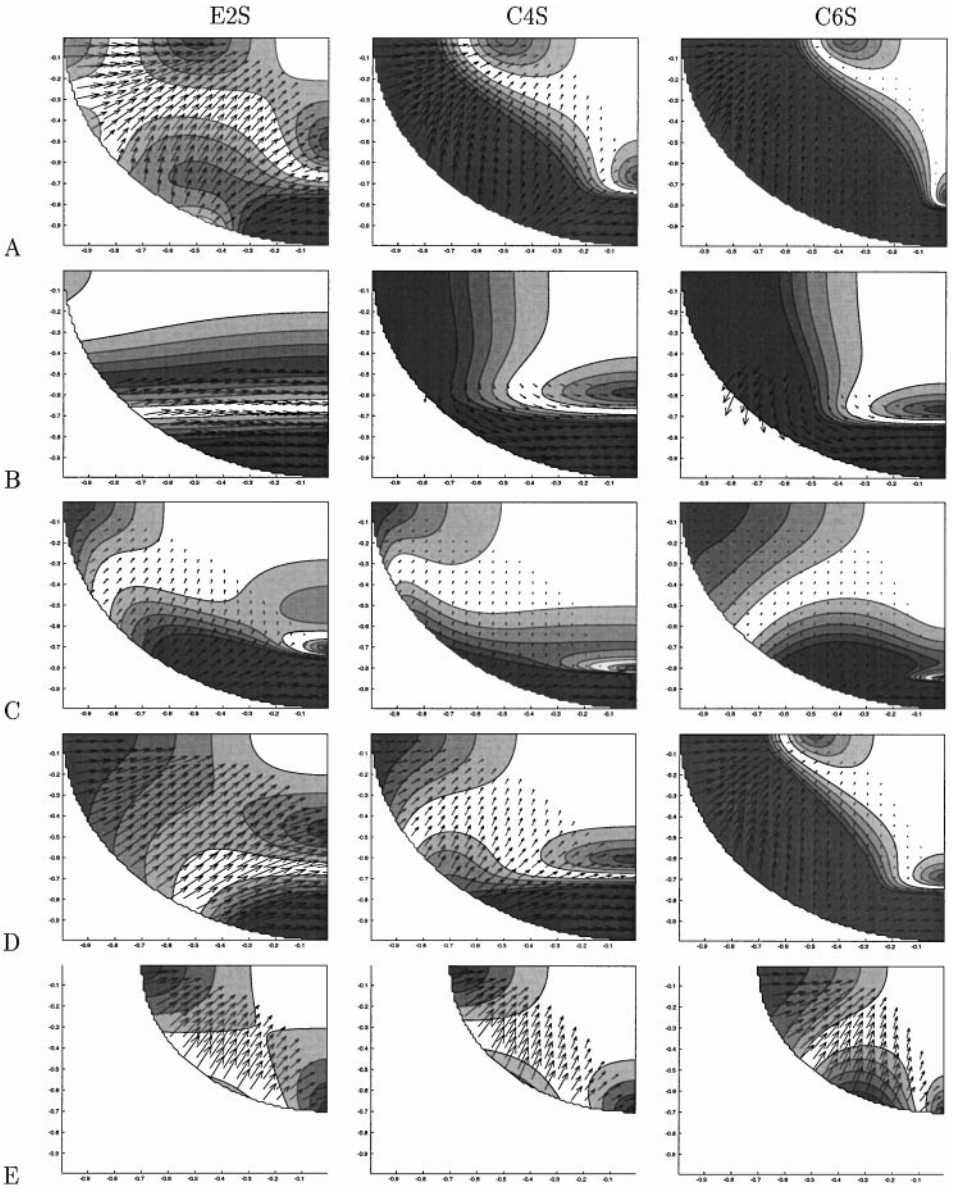

FIG. 10. Same as Fig. 9, for $\lambda/d = 0.25$.

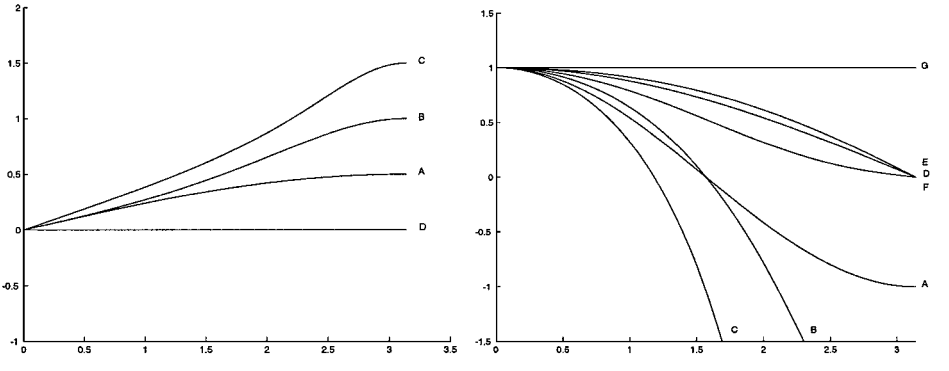

FIG. 11. First-order transfer functions of exact and approximate operators described in Table II. Left: R_0 for E2S (A), C4S (B), C6S (C), and exact interpolation (D). Right: R_1 for E2S (A), C4S (B), C6S (C); $R_{1/2}$ for E2S (D), C4S (E), C6S (F), and exact derivation (G).

6. CONCLUSION

We have derived a general approach for expressing the discrete dispersion relationships corresponding to inertia–gravity and Rossby waves on a computation grid, independent of the finite difference schemes. These relationships only involve the transfer functions of the schemes.

We have used this approach to investigate the interest of two families of compact schemes with regard to the conventional explicit second-order schemes. For inertia–gravity waves, the quality of the approximation of the dispersion relationship increases with the order of the schemes. The general patterns of the frequency and the group velocity remain identical, but with an increased accuracy. B and C grids are still the best choices for representing these waves whatever the family of schemes, but the domains of accuracy corresponding to all grids are very much enlarged when C4S or C6S are used rather than E2S. Note, however, that the use of compact schemes does not prevent the existence of numerical modes.

Concerning Rossby waves, the dispersion relationship involves not only the zero-order TFs but also the first-order TFs, the accuracies of which globally decrease with the order of the schemes. For that reason, C6S is less appropriate than C4S. However the use of C4S leads to clear improvement with regard to E2S in nearly all cases. In particular, it improves greatly the performance of the widely used C grid in the resolved case, which was one of the main failures of E2S.

In summary, the family of schemes C4S appears to be a good compromise for representing inertia–gravity and Rossby waves in ocean models. The present study should be followed by an evaluation of the performance of these schemes in representing the other important class of ocean waves, namely the coastal trapped Kelvin waves, and more generally in the context of a full ocean general circulation model, which will be the second part of this work.

ACKNOWLEDGMENTS

This work was supported by the French MERCATOR program. IDOPT is a joint CNRS/University of Grenoble/Institut National Polytechnique de Grenoble/INRIA project. The author thanks Dr. Alistair Adcroft for his helpful comments on this work.

REFERENCES

1. A. J. Adcroft, *Numerical Algorithms for Use in a Dynamical Model of the Ocean*, Ph.D. thesis (University of London, 1995).
2. A. Arakawa and V. R. Lamb, Computational design of the basic dynamical processes of the UCLA general circulation model, in *Methods of Computational Physics* (1977), Vol. 17.
3. P. C. Chu and C. Fan, A three-point combined compact difference scheme, *J. Comput. Phys.* **140**, 370 (1998).
4. L. Collatz, *The Numerical Treatment of Differential Equations* (Springer-Verlag, New York, 1966).
5. J. K. Dukowicz, Mesh effects for Rossby waves, *J. Comput. Phys.* **119**, 188 (1995).
6. M. Fox-Rabinovitz, Computational dispersion of horizontal staggered grids for atmospheric and ocean models, *Mon. Weather Rev.* **119**, 1624 (1991).
7. A. E. Gill, *Atmosphere–Ocean Dynamics* (Academic Press, San Diego, 1982), p. 496.
8. D. B. Haidvogel and A. Beckmann, *Numerical Ocean Circulation Modeling*, Series on Environmental Science and Management (Imperial College Press, London, 1999), Vol. 2.
9. S. K. Lele, Compact finite difference schemes with spectral-like resolution, *J. Comput. Phys.* **103**, 16 (1992).
10. Y. Song and T. Tang, Dispersion and group velocity in numerical schemes for three-dimensional hydrodynamic equations, *J. Comput. Phys.* **105**, 72 (1993).
11. R. C. Wajsowicz, Free planetary waves in finite-difference numerical models *J. Phys. Oceanogr.* **16**, 773 (1986).